communications physics

ARTICLE

https://doi.org/10.1038/s42005-022-00829-y OPEN

Optical excitations of Skyrmions, knotted solitons, and defects in atoms

Christopher D. Parmee[1]✉, Mark R. Dennis[2] & Janne Ruostekoski[1]✉

Analogies between non-trivial topologies of matter and light have inspired numerous studies, including defect formation in structured light and topological photonic band structures. Three-dimensional topological objects of localised particle-like nature attract broad interest across discipline boundaries from elementary particle physics and cosmology to condensed matter physics. Here we propose how simple structured light beams can be transformed into optical excitations of atoms with considerably more complex topologies representing three-dimensional particle-like Skyrmions. This construction can also be described in terms of linked Hopf maps, analogous to knotted solitons of the Skyrme-Faddeev model. We identify the transverse polarisation density current as the effective magnetic gauge potential for the Chern-Simons helicity term. While we prepare simpler two-dimensional baby-Skyrmions and singular defects using the traditional Stokes vectors on the Poincaré sphere for light, particle-like topologies can only be achieved in the full optical hypersphere description that no longer discards the variation of the total electromagnetic phase of vibration.

[1] Department of Physics, Lancaster University, Lancaster LA1 4YB, UK. [2] School of Physics and Astronomy, University of Birmingham, Birmingham B15 2TT, UK. ✉email: c.parmee@lancaster.ac.uk; j.ruostekoski@lancaster.ac.uk

Topologically non-trivial defects, textures, and knots have inspired physicists since the days of Kelvin[1]. They are remarkably ubiquitous throughout physics, spanning a vast range of energy scales from cosmology and elementary particle physics, to superconductors, superfluidity, and liquid crystals. The universal nature of topological stability in such diverse areas provides unprecedented opportunities to use experimentally accessible laboratory systems as emulators even of cosmology and high-energy physics where the experimental evidence is absent[2]. In recent years, the experimental study of topological defects and textures in structured optical fields has emerged as one of the most promising areas to engineer and detect topologically non-trivial characteristics[3], including singularities of the phase or polarisation that may form knotted or linked geometries[4–7] or Möbius strips[8]. Another line of research on non-trivial topologies of light has focused on photonic band structures[9], analogous to electronic band structures in crystals.

Topological Skyrmionic textures[10] are non-singular, localised spin (or pseudo-spin) configurations that do not perturb the spin profile sufficiently far from the centre of the structure. The non-trivial topology of the object arises from how the spatial profile of the spin texture wraps over the spin configuration, or order parameter, space. Particle-like Skyrmions, defined by mappings of the Π_3 homotopy group, display non-trivial three-dimensional (3D) spatial profiles and are well-known in nuclear and elementary particle physics as theoretical paradigms[11–14]. Similar structures have been proposed in cosmological models[15], and they have also been actively investigated in superfluids[16–19], with a particular focus on their energetic stability[20–24]. Hopfions, classified by the integer-valued Hopf charge, are closely related to the 3D Skyrmions and have attracted particular attention owing to their tendency to form stable torus knots[25–29]. Although 3D Skyrmions and Hopfions have recently been experimentally realised as stationary superfluid configurations[30,31], in liquid crystals[32], and in phase and polarisation-structured light[33], the wider attention has focused on much simpler, planar analogues, 2D baby-Skyrmions. 2D baby-Skyrmions, like their 1D cousins[34], exhibit topologically non-trivial non-singular configurations in reduced dimensions and have the best known early examples in superfluids as the Anderson-Toulouse-Chechetkin[35,36] and Mermin-Ho[37] non-singular vortices, owing to their ability to carry angular momentum. A large body of more recent research has included magnetic systems[38,39], with potential data storage applications, rotating atomic superfluids[40–47], exciton-polariton structures[48–51], and optical fields[52–55].

For the particular case of baby-Skyrmions in optical fields, field profiles are usually analysed using the Stokes vector, i.e., a point on the Poincaré sphere, corresponding to the coherent, transverse polarisation state at each point in the field. However, going beyond these more easily observable parameters, the full topology of the field configurations, crucially, also depends on the spatial variation of the total phase of vibration on the polarisation ellipse[56], which is the sum of the phases of the electric field components, and is not represented by the Stokes vector. This complete topology is then described by the optical hypersphere S^3 (unit sphere in 4D)[33], allowing, e.g., for full 3D particle-like topologies of light.

Here we utilise simple configurations of structured light fields to show how these can lead to optical excitations in atomic media of comparable or considerably more complex topologies. Baby-Skyrmions, represented by full Poincaré beams[57] in light fields, can straightforwardly be transferred to optical excitations and therefore frozen and stored in strongly confined oblate atomic ensembles. We consider a $J = 0 \rightarrow J' = 1$ transition that can form, e.g., in ^{88}Sr very long-lived excitations. By going beyond the Stokes representation of light beams to incorporate the full degrees of freedom of the complex field amplitudes, where we no longer discard the spatial variation of the sum of the phases for the two field components, we can form 3D particle-like Skyrmions, localised in space. We identify the transverse polarisation density of the atoms as a synthetic magnetic vector potential of the 3D Skyrmions with non-trivial helicity. While constructing such an object directly in a light beam is quite challenging even for modern structured light engineering[33], we show how appropriately adjusting the light-matter coupling provides a solution with simple copropagating beams. For this solution, we then formulate the Stokes representation to provide precisely a Hopf fibration between the optical hypersphere and the Poincaré sphere, representing knotted solitons or Hopfions, analogous to the knotted solitons in the Skyrme-Faddeev model[11,25], and show the linked and trefoil knot Hopfion preimages of the Poincaré sphere. While such objects are non-singular, we also show how singular defects can be transferred from light to optical excitations in oblate atomic ensembles. For systems where the light scattering is strong, and light mediates dipole-dipole interactions between the atoms, we remarkably find that singular defects can even exist as collective excitation eigenmodes. These behave as spatially delocalised "superatoms", exhibiting their own collective resonance linewidth and line shift.

Results

Baby-Skyrmions. We first show how to prepare 2D baby-Skyrmions in an oblate atomic ensemble, strongly confined to a region smaller than the atomic transition wavelength along the z-direction. A non-singular topological texture can be constructed by having a (pseudo-)spin order parameter which orients into a localised structure pointing in every direction somewhere within a 2D plane, and is well-defined at each point to be a non-singular texture. The order parameter takes a uniform constant value everywhere sufficiently far away from the origin, independently of the direction, and so the plane can then be compactified to a unit sphere S^2 and the orientations of the spin on the 2D plane can be characterised by $S^2 \rightarrow S^2$ mappings. Such mappings can take topologically non-trivial values, associated with the existence of baby-Skyrmions, also frequently called non-singular (or coreless) vortices.

For optical fields, the state is most commonly characterised on the S^2 Poincaré sphere by an easily observable Stokes vector $\mathbf{S}$[56,58], and the $S^2 \rightarrow S^2$ mapping defining the baby-Skyrmion topology counts the number of times the object wraps over S^2:

$$W = \int_{\mathcal{S}} \frac{d\Omega_i}{8\pi} \epsilon_{ijk} \mathbf{S} \cdot \frac{\partial \mathbf{S}}{\partial r_j} \times \frac{\partial \mathbf{S}}{\partial r_k}, \tag{1}$$

where r_j denotes the real space coordinates, ϵ_{ijk} a completely antisymmetric Levi-Civita tensor and $d\Omega_i$ an area element of a surface $\mathcal{S}$ that covers the full texture in real space. A field configuration that satisfies a non-trivial winding $W = 1$ can be achieved using a superposition of a Gaussian and Laguerre-Gaussian (LG) beam, with wavevector $\mathbf{k}$ and frequency $\omega = c|\mathbf{k}| = ck$. Working with slowly-varying amplitudes for the light and atoms by factoring out the fast-rotating term $\exp(-\mathrm{i}\,\omega t)$, the positive frequency component of the field, $\boldsymbol{\mathcal{E}}(\mathbf{r})$, is given by:

$$\boldsymbol{\mathcal{E}}(\mathbf{r}) = U_{0,0}(w_0)\hat{\mathbf{e}}_x + U_{1,0}(w_0)\hat{\mathbf{e}}_y. \tag{2}$$

Here $U_{l,f}(w_0)$ are the LG modes with azimuthal quantum number l, radial quantum number f, and focused beam width w_0[3]. The light field of Eq. (2), now a full Poincaré beam[57], contains a Néel type baby-Skyrmion whose optical polarisation we have defined here in the linear $\hat{\mathbf{e}}_{x,y}$ basis, instead of the commonly used circular basis[49,54,55], because the linear basis is convenient to work with so the Stokes vector representation can be defined to coincide with

the Hopf fibration, as discussed in the "Particle-like objects: 3D Skyrmions" section.

Topologically non-trivial fields in this simple example can be straightforwardly transformed to optical excitations in atomic ensembles. We consider a $|J=0,m=0\rangle \rightarrow |J'=1,m=\mu\rangle$ transition which can be very narrow in alkaline-earth-metal-like atoms, forming long-lived excitations. For instance, the ^{88}Sr clock transition $^1S_0 \rightarrow {}^3P_0$ has a linewidth controllable by a magnetic field, with the transition entirely forbidden at the zero field. We create a non-singular topological texture of the optical excitation by considering an oblate ensemble of atoms, strongly confined along the light propagation direction (z-axis). We write the optical excitation as an electric polarisation density, or the density of electromagnetic vibration in atoms, with the slowly-varying positive frequency component $\mathbf{P}(\mathbf{r}) = \sum_j \delta(\mathbf{r}-\mathbf{r}_j)\mathbf{d}_j$. The induced dipole $\mathbf{d}_j = \mathcal{D}\sum_\mu \hat{\mathbf{e}}_\mu \mathcal{P}_\mu^{(j)}$ on atom j, located at $\mathbf{r}_j$, is given in terms of the reduced dipole matrix element $\mathcal{D}$ and the complex excitation amplitudes $\mathcal{P}_\mu^{(j)}$, with the unit vectors $\hat{\mathbf{e}}_\pm = \mp(\hat{\mathbf{e}}_x \pm \mathrm{i}\,\hat{\mathbf{e}}_y)/\sqrt{2}$ and $\hat{\mathbf{e}}_0 = \hat{\mathbf{e}}_z$. The incident light $\boldsymbol{\mathcal{E}}(\mathbf{r})$ excites a polarisation density $\mathbf{P}(\mathbf{r}) = \epsilon_0 \alpha \boldsymbol{\mathcal{E}}(\mathbf{r})$ in the atoms via the atomic polarisability, $\alpha = -\mathcal{D}^2/[\hbar\epsilon_0(\Delta + \mathrm{i}\,\gamma)]$ (see "Methods"), where γ denotes the resonance linewidth of the atom and Δ is the detuning of the laser frequency from the atomic resonance. The excitation is then re-emitted and detectable in the transmission of the total field, $\mathbf{E}(\mathbf{r}) = \boldsymbol{\mathcal{E}}(\mathbf{r}) + \mathbf{E}_{\mathrm{sc}}(\mathbf{r})$, where the scattered light amplitude is given by $\epsilon_0 \mathbf{E}_{\mathrm{sc}}(\mathbf{r}) = \int d^3r' \mathsf{G}(\mathbf{r}-\mathbf{r}')\mathbf{P}(\mathbf{r}')$, and $\mathsf{G}(\mathbf{r})\mathbf{d}$ denotes the radiation at $\mathbf{r}$ from an oscillating dipole $\mathbf{d}$ at the origin, with G the dipole radiation kernel[59].

For describing the topology of the optical excitation, we define a pseudo-spinor in terms of the complex, normalised transverse atomic polarisation densities:

$$\hat{\mathsf{P}}(\mathbf{r}) = \begin{pmatrix} \hat{P}_x(\mathbf{r}) \\ \hat{P}_y(\mathbf{r}) \end{pmatrix}, \tag{3}$$

where, as for the light field in Eq. (2), we work in a linear rather than circular basis, with $\hat{P}_j = P_j/|\mathbf{P}|$ and the longitudinal component $P_z = 0$. We can then define the corresponding atomic Stokes vector:

$$S_j(\mathbf{r}) = \hat{\mathsf{P}}^\dagger \sigma_j \hat{\mathsf{P}}, \tag{4}$$

where σ_j are the Pauli matrices. In Fig. 1, we show the baby-Skyrmion configuration generated by the field in Eq. (2). The atomic Stokes vector, Eq. (4), now has a fountain-like structure $\mathbf{S} = [2\sqrt{2}\rho w_0 \hat{\mathbf{e}}_\rho + (w_0^2 - 2\rho^2)\hat{\mathbf{e}}_z]/(w_0^2 + 2\rho^2)$, with $\mathbf{S}$ written in a cylindrical polar basis $\hat{\mathbf{e}}_\rho$ and $\hat{\mathbf{e}}_z$, and takes a uniform value $\mathbf{S} = -\hat{\mathbf{e}}_z$ sufficiently far away from the centre of the object. It is easy to verify that the winding number Eq. (1) for $\mathbf{S}$ integrates to $W = 1$, and that the same topological structure in the incident field is excited in the atomic polarisation density, which could be detected in experiment with near-field imaging. The principle of creating a baby-Skyrmion is therefore closely related to the studies of analogous objects in exciton-polariton systems[48,49].

Particle-like objects: 3D Skyrmions. We now show how 3D Skyrmionic structures can be constructed in non-oblate atomic ensembles by considering the full complex nature of the electric polarisation. The Stokes vector representation of the Poincaré sphere for the light field amplitudes or optical excitations in atoms (Eq. (4)) does not provide the full field description, as the texture may also exhibit non-trivial, non-uniform spatial variation of the total phase of the two field components, which is discarded. A more complete description of the field topology can instead be obtained using the optical hypersphere[33] S^3.

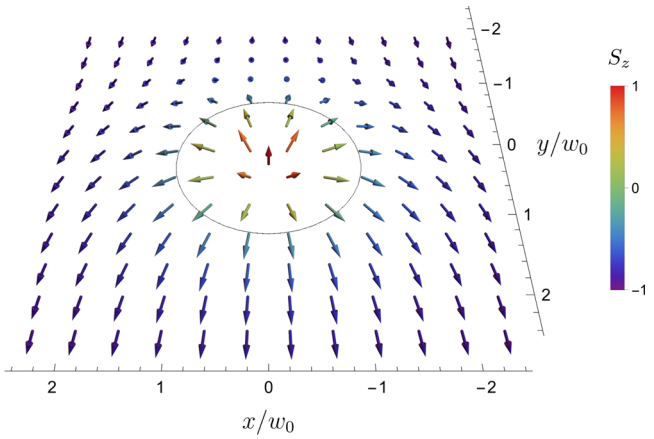

Fig. 1 Optical excitation of a baby-Skyrmion. The baby-Skyrmion has a characteristic fountain-like structure in the atomic Stokes vector $\mathbf{S}$ (Eq. (4)), generated by the light field of Eq. (2), with beam width w_0. $\mathbf{S}$ points along the z ($-z$) direction at the origin (large distances from the origin), and lies in-plane at the radius $\rho = w_0/\sqrt{2}$ (black circle), corresponding to the poles and equator of the Poincaré sphere, respectively. For illustrative purposes, we choose a regular square array for the atomic ensemble, but any geometry can be chosen.

The field parametrisation in S^3 permits considerably more complex, particle-like objects, localised in 3D physical space, which can be characterised by a corresponding higher-dimensional spin order parameter. Compactifying the real 3D space, such that the order parameter is assumed to take the same value far away from the particle, independently of the direction, allows us to describe the topology by $S^3 \rightarrow S^3$ mappings. Such mappings can be characterised by distinct topological equivalence classes, identified by the third homotopy group elements $\Pi_3(S^3) = \mathbb{Z}$. Non-trivial objects whose S^3 mappings wrap over the order parameter space an integer number of times represent topologically non-trivial solutions, originally introduced by Skyrme[10].

We now parametrise the atomic polarisation spinor Eq. (3) on the S^3 optical hypersphere by writing it as a four-component unit vector $\hat{\mathbf{n}} = (n_1, n_2, n_3, n_4)$, and taking:

$$\hat{\mathsf{P}} = \begin{pmatrix} n_2 + \mathrm{i}\,n_1 \\ n_4 + \mathrm{i}\,n_3 \end{pmatrix} = \begin{pmatrix} \mathrm{i}\sin\psi\sin\beta\exp(-\mathrm{i}\,\eta) \\ \cos\psi + \mathrm{i}\,\sin\psi\cos\beta \end{pmatrix}, \tag{5}$$

where $\hat{\mathbf{n}}$ is represented by the hyperspherical angles $0 < \psi \le \pi$, $0 < \beta \le \pi$ and $0 < \eta \le 2\pi$. The integer topological charge, B, of the 3D Skyrmion (known in high-energy physics as the baryon number[14]), is found then by counting the number of times $\hat{\mathbf{n}}$ wraps over S^3:

$$B = \int d^3r \mathcal{B}(\mathbf{r}) = -\int \frac{d^3r}{2\pi^2} \epsilon_{ijk}\epsilon_{abcd} n_a \frac{\partial n_b}{\partial r_i}\frac{\partial n_c}{\partial r_j}\frac{\partial n_d}{\partial r_k}, \tag{6}$$

where $\mathcal{B}(\mathbf{r})$ is the topological charge density. By introducing the transverse polarisation density current $\mathbf{J} = \frac{1}{2\mathrm{i}}[\hat{\mathsf{P}}^\dagger \nabla \hat{\mathsf{P}} - (\nabla \hat{\mathsf{P}}^\dagger)\hat{\mathsf{P}}]$, $\mathcal{B}$ can be rewritten as:

$$\mathcal{B}(\mathbf{r}) = -\frac{1}{4\pi^2}\mathbf{J}\cdot\nabla\times\mathbf{J}, \tag{7}$$

and is therefore analogous to the linking number density in (super)fluids[16], where $\mathbf{J}$ is replaced by the (super)fluid velocity, and to the Chern-Simons term for the magnetic helicity[60], in which case $\mathbf{J}$ represents the gauge potential for the magnetic field (note that the sign of the winding numbers may vary depending

on the orientations of the coordinates and the mappings). To understand the structure of the Skyrmion in Eq. (5), we consider a simple analytic mapping from 3D Euclidean real space, with spherical polar coordinates (r, ϕ, θ), to the optical hypersphere[22] with $\psi = q\varsigma(r)$, $\beta = \theta$ and $\eta = p\phi$. We find that Eq. (6) integrates to give a topological charge $B = pq$, where the monotonic function $\varsigma(r)$ satisfies $\varsigma(0) = 0$ and $\varsigma \to \pi$ sufficiently far from the origin. The first spinor component, $\hat{P}_x$, vanishes along the z-axis, and now forms a multiply-quantised vortex line with a winding number p. The second component, $\hat{P}_y$, vanishes at the circles $\theta = \pi/2$, $r = \varsigma^{-1}[(n - 1/2)\pi/q]$ for $n = 1, \ldots, q$, and forms q concentric vortex rings with different radii where Taylor expanding to first order gives $\hat{P}_y \sim -\delta r - \mathrm{i}\,\delta\theta$ in the circle vicinity. The vortex line threads the vortex rings, and has a non-vanishing density confined inside the toroidal regions around the vortex ring singularities, such that the Skyrmion is spatially localised, forming a particle-like object. Any continuous deformation of the Skyrmion structure in Eq. (5) conserves the discrete topological charge; a 3D Skyrmion with $B = pq$ can also be constructed by taking any combination of singly- and multiply-quantised lines (rings) with total winding p (q), located in the components of $\hat{P}_x$ ($\hat{P}_y$), where the lines thread through the rings.

Forming such a structure in the polarisation density using electromagnetic fields in free space alone is a rather challenging task of structured light engineering[33]. However, we can here exploit the properties of the light-matter coupling to simplify the field profiles considerably. To create the Skyrmion, we take a coherent superposition of copropagating light beams:

$$\boldsymbol{\mathcal{E}}(\mathbf{r}) = U_{l,0}(w_0)\hat{\mathbf{e}}_x + [U_{0,0}(w_1) - cU_{0,0}(w_2)]\hat{\mathbf{e}}_y, \tag{8}$$

where for the LG beam we now choose $l = 1$ to form a $B = 1$ Skyrmion, although we consider higher-order charges in the next section. For the Gaussian beams of unequal focusing, the parameter $c = \exp(-\rho_0^2/w_1^2 + \rho_0^2/w_2^2)$ defines the circular radius ρ_0 in the $z = 0$ plane of minimum focusing at which they interfere destructively. Destructive interference outside the ring is prevented due to diffraction. Diffraction also leads to variation of the phase (Gouy phase), such that $U_{0,0}(w_1) - cU_{0,0}(w_2) \sim (\rho - \rho_0) + \mathrm{i}\zeta z$ in the zero field ring vicinity. The y-polarised light component now forms a singular vortex ring[61] with a 2π phase winding, analogously to $\hat{P}_y$ of Eq. (5) for $q = -1$, and a vortex core anisotropy along the z-direction:

$$\zeta = \frac{w_1^2 w_2^2 - \rho_0^2(w_1^2 + w_2^2)}{w_1^2 w_2^2 \rho_0 k}. \tag{9}$$

The x-polarised light component exhibits a singular vortex line, analogously to $\hat{P}_x$ of Eq. (5) for $p = -1$, where the LG beam has an intensity that reaches its maximum in the $z = 0$ plane at $\rho = w_0/\sqrt{2}$, chosen to coincide with the vortex ring singularity. However, the intensity of the beam, and hence P_x, is not confined along the beam propagation direction as required by the Skyrmion solution Eq. (5). In order to obtain the desired profile, we can alter the light-matter coupling of the atoms selectively around the $z = 0$ plane, which then modifies P_x so it decays quickly along the z-direction of the atomic ensemble. This can be achieved by controlling the $m = 0$ quadratic Zeeman level shift, either by magnetic fields, or ac Stark shifts of lasers or microwaves[62].

In Fig. 2a, we show the topological charge density $\mathcal{B}$ for the 3D Skyrmion constructed using the field in Eq. (8), [ignoring any contribution from the beam phase factor $\exp(\mathrm{i}\,kz)$], and the confinement of P_x, achieved using spatially dependent level shifts $\Delta_x(\mathbf{r}) = \delta[1 - \exp(-z^2/10w_0^2)]$ in $\mathbf{P}(\mathbf{r}) = \epsilon_0\alpha(\Delta_\mu)\boldsymbol{\mathcal{E}}(\mathbf{r})$ (see "Methods"). We consider long-lived excitations with extremely narrow linewidths, so typically $\delta \gg \gamma$, and we take $\delta/\gamma = 200$. The topological charge density shows the localisation of the Skyrmion, with the density concentrated at the origin, and also in two rings where the gradient of P_x and P_y becomes large from the applied level shifts and vortex ring phase winding, respectively. Changing the vortex ring core anisotropy, Eq. (9), which has the value $\zeta = 0.08$ in Fig. 2a, increases the concentration in the rings for a more anisotropic core. We find the corresponding transverse polarisation density current $\mathbf{J}$ [Fig. 2b], which represents the synthetic magnetic vector potential with an integer linking number, has a large magnitude where the charge density is highly concentrated. At the charge density rings, $\mathbf{J}$ flows radially inwards or outwards, while closer to the origin, $\mathbf{J}$ flows almost entirely along the $\pm x$ directions.

Particle-like objects: knotted solitons. We have shown how 3D particle-like objects can be prepared by going beyond the Stokes vector representation used to describe baby-Skyrmions in the "Baby-Skyrmions" section and parametrising the optical excitations on S^3. However, we can also construct particle-like 3D objects using the Poincaré sphere, instead of the full optical hypersphere. The advantages of our choice of representation for the optical hypersphere in Eq. (5) become apparent when we formulate the $S^3 \to S^2$ transformation from the optical hypersphere to the Stokes vector precisely as a Hopf fibration[33,63].

The Hopf fibration, initially of purely mathematical interest, arises naturally in field theories. In the Skyrme-Faddeev model, 3D topological objects known as Hopfions are classified by an integer-valued Hopf charge[25–29]. Considerable interest in these systems was generated by the observations that the stable solutions may exhibit knots. The Hopf map of the vector $\hat{\mathbf{n}}$ on S^3 to a vector $\hat{\mathbf{h}} = (h_1, h_2, h_3)$ on S^2 is given by:

$$h_1 = 2(n_1 n_3 + n_2 n_4), \tag{10}$$

$$h_2 = 2(n_2 n_3 - n_1 n_4), \tag{11}$$

$$h_3 = n_1^2 + n_2^2 - n_3^2 - n_4^2, \tag{12}$$

where the mapping falls into distinct topological equivalence classes $\Pi_3(S^2) = \mathbb{Z}$, characterised by the integer Hopf charge, Q_H. Upon substituting the expressions for $\hat{\mathbf{n}}$ in terms of $\hat{\mathbf{P}}$, the mapping indeed returns the atomic Stokes vector, Eq. (4). Applying the Hopf map of Eqs. (10)–(12) to the $B = 1$ Skyrmion of Fig. 2a, we obtain a Hopfion with charge $Q_\mathrm{H} = 1$, shown in Fig. 2c by the field profile $\hat{\mathbf{h}}$. The particle-like nature of the Hopfion is clearly visible, where the full 3D spin texture is localised around the origin. At large distances in any direction from the centre, and along the vortex line where $\hat{P}_x$ vanishes, we have $\hat{\mathbf{h}} = (0, 0, -1)$, while at the vortex ring with $\hat{P}_y = 0$, $\hat{\mathbf{h}} = (0, 0, 1)$.

The topological structure of the Hopfion is revealed when considering the reduction in dimensionality of the parameter space under the Hopf map of Eqs. (10)–(12), where multiple points on S^3 map to the same point on S^2. These points form closed curves in real space, known as Hopfion preimages, which interlink an integer number of times, as the preimages of the Hopfion introduced in Fig. 2c show in Fig. 3a. The linking number is given by the Hopf charge, Q_H, which can be shown[64] to be equal to the 3D Skyrmion charge, Eq. (6). Therefore, we can increase the preimage interlinking by increasing the total winding of vortex rings and lines, as discussed in the "Particle-like objects: 3D Skyrmions" section. Multiply-quantised vortex lines in P_x can easily be prepared by changing the beam orbital angular momentum in Eq. (8). Choosing $l = 2$, we form

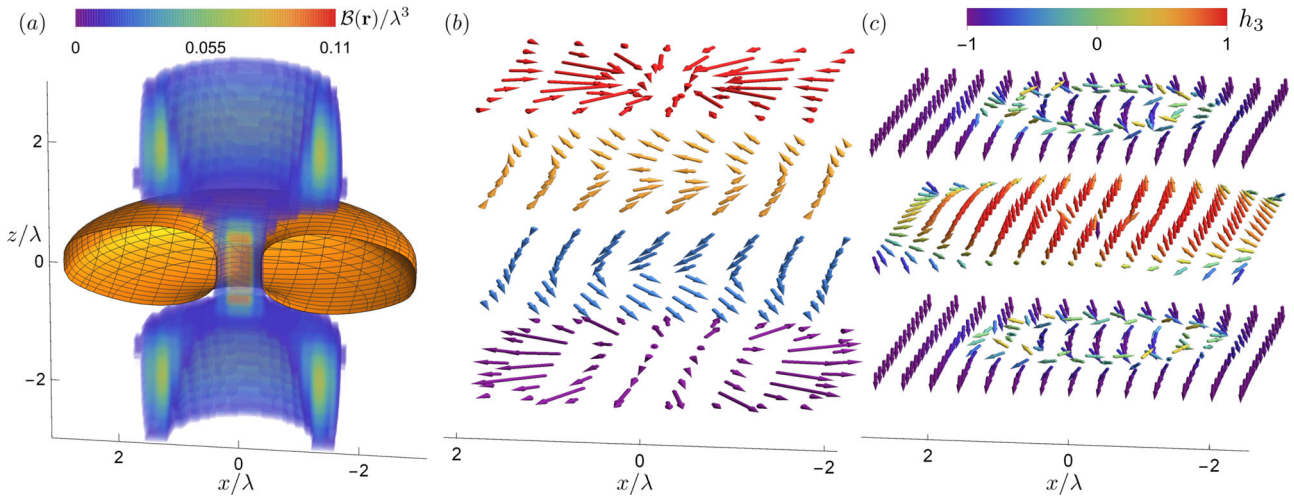

Fig. 2 Topological particle-like objects of optical excitations. a A 3D Skyrmion with the topological charge $B = 1$, prepared using the light field in Eq. (8) for $l = 1$; **b** its artificial gauge vector potential field, represented by the polarisation density current **J**; and **c** the construction of the Hopfion field profile $\hat{\mathbf{h}}$. **a** The confinement of the x-polarised electromagnetic vibration of the atoms, $P_x(\mathbf{r})$, due to the applied level shifts is shown by the isosurface $|P_x(\mathbf{r})|^2 = 0.6\mathcal{D}^4|\mathcal{E}(\mathbf{0})|^2/(\hbar\gamma)^2$ (meshed region). The topological charge density $\mathcal{B}(\mathbf{r})$ (coloured region) is concentrated at the origin and in two rings where the gradients of the atomic polarisation density become large, with the corresponding **J** in **b** exhibiting a flow in the $\pm x$ directions near the origin or radial flow at the charge density rings. In **b**, **c**, a geometry of stacked square arrays is chosen for illustrative purposes, although any geometry can be used. All figures use the same z-axis. In **b**, the atomic planes lie at $z/\lambda = \pm 2.5$ and $z/\lambda = \pm 0.83$, and in **c** lie at $z = 0$ and $z/\lambda = \pm 2$. The beam widths $(w_0, w_1, w_2)/\lambda = (2, 3, 4.5)$.

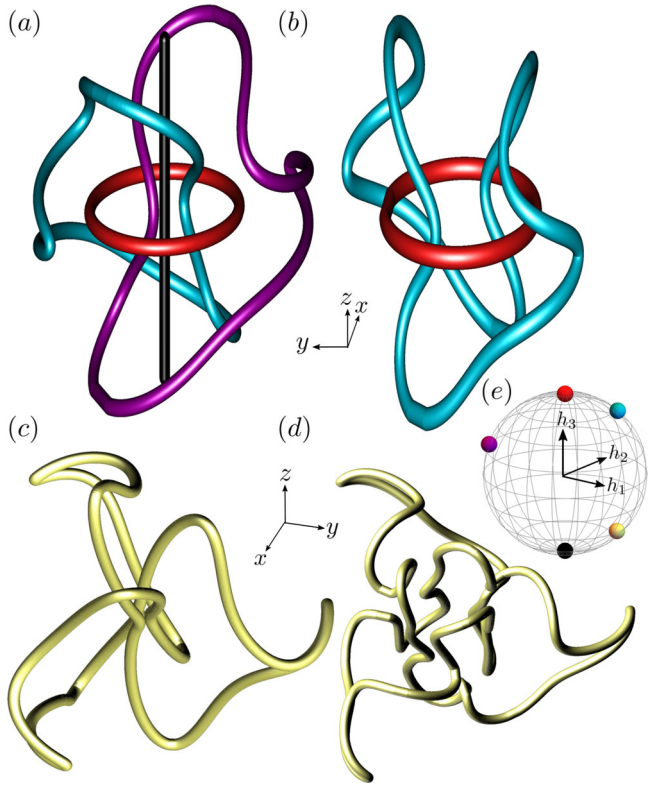

Fig. 3 Links and knots in particle-like Hopfion optical excitations. a–**d** Real space preimages of Hopfions with different Hopf charge, Q_H, where each preimage corresponds to a point on the Poincaré sphere S^2 (**e**). Hopfion with **a** $Q_H = 1$, **b** $Q_H = 2$, where preimages interlink once and twice, respectively, and organise around the preimages of the vortex ring (red circle) and vortex line (black line corresponding to a circle of infinite radius). **c**, **d** $Q_H = 6$ Hopfions with trefoil knot preimages. The Hopfions are created using the light field in Eq. (8) with l equal to **a** 1, **b** 2, **c**, **d** 3, and the y-polarised light component replaced in **c** by a two-photon transition and in **d** by the LG beams of Eq. (13). The beam widths $(w_0, w_1, w_2)/\lambda = (2, 3, 4.5)$.

a $Q_H = 2$ Hopfion with real space preimages that interlink twice, as shown in Fig. 3b.

Here we show how we can even prepare Hopfions that have the highly sought-after knotted structure[25–28] where each preimage is itself a knot, provided that the total winding of vortex rings is increased. This is more complicated than preparing higher quantised vortex lines, not least because multiply-quantised optical vortex rings are forbidden in paraxial light beams[65]. However, we overcome this limitation by two alternative strategies. The first is to create the Hopfion using the field in Eq. (8), but where the y-polarised light component is now chosen to drive a two-photon transition, with the beam wavelength doubled. Each photon excites a single vortex ring, such that $P_y \propto [U_{0,0}(w_1) - cU_{0,0}(w_2)]^2$, therefore forming a doubly-quantised ring[61], where $P_y \sim [(\rho - \rho_0) + i\zeta z]^2$ in the ring vicinity. Using then $l = 3$ for the LG beam in Eq. (8) to prepare a triply-quantised vortex line that threads the vortex ring, we create a Hopfion that has a real space preimage of a trefoil knot, Fig. 3c. An alternative method is to choose the y-polarised light component in Eq. (8) to be structured according to the techniques of refs. [4,65], where using the superposition of LG modes:

$$\mathcal{E}_y(\mathbf{r}) \simeq 0.25U_{0,0}(w_0) - 0.6U_{0,1}(w_0) + 0.375U_{0,2}(w_0), \qquad (13)$$

gives a configuration of four coaxial vortex rings (two oppositely winding in the focal plane, one above and one below the focal plane), through which the triply-quantised vortex line threads and creates a Hopfion with a trefoil knot preimage, Fig. 3(d).

The scattered light from the Hopfion and $\hat{\mathbf{h}}$ both depend on $\hat{P}_x$ and $\hat{P}_y$, with light emitted from atoms with different $\hat{\mathbf{h}}$ having different spatial profiles and polarisations, e.g., atoms with $\hat{P}_y = i\hat{P}_x$ ($\hat{P}_y = \hat{P}_x$) where $\hat{\mathbf{h}} = (0, 1, 0)$ [$\hat{\mathbf{h}} = (1, 0, 0)$] will have circular (linear) polarisation along the z-direction. Therefore, by calculating the expected light profile from the ensemble and comparing to experimental readings, we gain information about the order parameter. To determine the Hopfion structure further, we can exploit the applied level shifts to constrain the polarisation density to a localised region in space where it would be

approximately constant and zero elsewhere. $\hat{P}_x$ and $\hat{P}_y$ could be altered by manipulating the $m=0$ and $m=+1$ level shifts, respectively, to observe the Hopfion preimages of Fig. 3 and their interlinking.

Singular defects. Until now, we have considered non-singular topological textures where the order parameter forming the texture is always well-defined throughout the atomic ensemble. We now show how it is also possible to form 2D singular defects (looking again at oblate atomic ensembles strongly confined along the z-direction), for which the spin and order parameter become ill-defined at a finite number of points. Structured light fields that exhibit singularities can create singular defects in atomic optical excitations by analogous principles to non-singular textures. To form 2D optical point defects, we consider a cylindrical beam profile[66] formed by a superposition of two LG beams with opposite orbital angular momenta in the circular polarisation basis[49]:

$$\boldsymbol{\mathcal{E}}(\mathbf{r}) = \mathrm{e}^{-\mathrm{i}\varphi/2}U_{1,0}(w_0)\hat{\mathbf{e}}_+ + \mathrm{e}^{\mathrm{i}\varphi/2}U_{-1,0}(w_0)\hat{\mathbf{e}}_-, \qquad (14)$$

where $\varphi=0$ ($\varphi=\pi$) results in an azimuthal (radial) singular vortex in the light field.

For a dominant incident field, the singular configuration can be transferred onto the atomic polarisation density without the need for any applied level shifts, as in the "Baby-Skyrmions" section. Such a configuration eventually radiates at the single-atom decay rate. However, remarkably, we find that specific defect structures can be highly robust and stable even in the strongly interacting limit where the incident field is no longer dominant in the atomic ensemble. These structures therefore represent spatially delocalised coherent "superatoms" that extend over the sample. In a cold and dense atomic ensemble, resonant incident light can scatter strongly, mediating dipole-dipole interactions between the atoms. In Fig. 4a, b, we show the real components of the steady-state polarisation density for interacting atoms driven by the field in Eq. (14), with $w_0/\lambda=2.77$, in the limit of low light intensity where individual atoms respond to light as classical linear oscillators[67,68]. For an atom spacing $a/\lambda=0.5$, the intensity of light scattered between nearest-neighbour atoms at the centre of the lattice, I_{scat}, is much larger than the maximum intensity of the incident field, I_{inc}, with $I_{\mathrm{scat}}/I_{\mathrm{inc}}\simeq 2$. Therefore the atoms no longer emit light independently, but instead exhibit collective optical excitations, together with collective resonance linewidths and line shifts. Despite the presence of strong collective behaviour, which we would expect to destabilise any structure imprinted by the light, the optical excitations in Fig. 4 show clear azimuthal and radial point vortex-like structures similar to the incident field. To understand this behaviour, we calculate the collective excitation eigenmodes of the interacting system (see "Methods" for details).

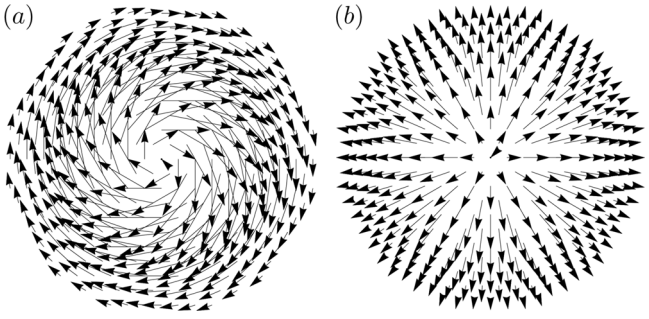

Fig. 4 Collective optical excitations with singular-like defects. The real component of the atomic polarisation density $\mathbf{P}(\mathbf{r})$ exhibits (**a**) an azimuthal or (**b**) radial point vortex in a steady-state response to the incident light field of Eq. (14) that mediates dipole-dipole interactions between the atoms in an $N=313$ triangular array with circular boundaries and spacing $a/\lambda=0.5$. The imaginary part of $\mathbf{P}(\mathbf{r})$ is approximately zero. The beam width $w_0/\lambda=2.77$, phase $\varphi=0$, and laser frequency detuning from the atomic resonance $\Delta/\gamma=0.90$ for **a**, or $\varphi=\pi$ and $\Delta/\gamma=0.89$ for **b**.

We find that the system supports several collective eigenmodes with singular defects in the real components of the complex atomic polarisation density amplitudes. The resulting stationary excitations in Fig. 4 consist almost solely of a single collective excitation with an azimuthal (radial) defect, with a well-defined resonance linewidth and line shift, where the eigenmode occupation reaches 99% at the eigenmode resonance, $\Delta/\gamma=0.90$ ($\Delta/\gamma=0.89$), and the excitation decays with a lifetime set by the collective linewidth, $\upsilon/\gamma=1.11$ ($\upsilon/\gamma=1.09$), in the absence of any incident field. $S^1\to S^1$ mappings determine the winding number (Poincaré index) for a singular topological defect, as the count of the net total change in the real components of the polarisation density orientation around a closed loop:

$$Q=\oint\frac{d\mathbf{r}}{2\pi}\cdot\nabla\arg\left(\hat{P}_x+\mathrm{i}\,\hat{P}_y\right), \qquad (15)$$

with $Q=1$ for the azimuthal and radial vortices. In an infinite system, the collective eigenmodes are real, and the system exhibits true topological defects. However, for the small atomic ensembles considered here, the imaginary components of the eigenmodes do not entirely vanish, e.g., the azimuthal vortex eigenmode appearing in the stationary excitation of Fig. 4a has a small 3% contribution to the total polarisation density amplitude from the imaginary part. In comparison, the full stationary excitation has a 2% contribution from the imaginary part.

Discussion

3D particle-like topological objects have inspired research across a wide range of different disciplines. The ideas originate from Kelvin, who proposed how vortex strings forming closed loops, links, and knots could explain the structure of atoms[1]. To transfer such universal concepts to light and optical excitations, standard textbook representations of field amplitudes in terms of the Stokes vector on the Poincaré sphere fall dramatically short of the goal. This is because particle-like topologies can only be achieved in the complete optical hypersphere description, where variation of the total electromagnetic phase of vibration is retained. Here we have constructed a comprehensive platform of topologically non-trivial optical excitations of atoms, induced by light. The resulting amplitudes of electronic vibrations have been shown to exhibit substantially more complex topologies than the incident light creating them. In addition, this allows topological objects to be stored in excitations in highly controllable quantum systems with long lifetimes.

The proposed setup potentially paves the way for applications in future quantum simulators. The Skyrme model of 3D particle-like objects[10] is not only an elegant mathematical construction, but also simulates a low-energy limit of quantum chromodynamics where baryons are described by the quantised states of classical soliton solutions[69]. By describing these field configurations using linked Hopf maps, the particle-like objects take the form of links and knots, analogous to knotted solitons of the Skyrme-Faddeev model[25–29], and representing physical realisations of Kelvin's ideas in optical excitations.

Methods

Light-matter coupling and collective excitation eigenmodes. To evaluate the effect of light-mediated interactions, we calculate the total field at each atom which is given by the sum of the incident field and the light scattered from every other atom. In the limit of low light intensity, we only retain terms to first order in $\mathcal{E}$ and $\mathcal{P}_\mu^{(j)}$. The

dynamics of the complex atomic polarisation amplitudes are then linear and can then be determined by the set of coupled equations[68], $\dot{\mathbf{b}} = \mathrm{i}\mathcal{H}\mathbf{b} + \mathbf{F}$, where $\mathbf{b}_{3j-1+\mu} = \mathcal{P}_\mu^{(j)}$, and $\mathbf{F}_{3j-1+\mu} = \mathrm{i}\xi\epsilon_0\hat{\mathbf{e}}_\mu^* \cdot \mathcal{E}(\mathbf{r}_j)/\mathcal{D}$, with $\xi = 6\pi\gamma/k^3$. The matrix $\mathcal{H}$ has diagonal elements $\Delta_\mu(\mathbf{r}_j) + \mathrm{i}\gamma$, while the off-diagonal elements are given by light-mediated dipole-dipole interactions between the atoms $\xi\hat{\mathbf{e}}_\mu^* \cdot \mathsf{G}(\mathbf{r}_j - \mathbf{r}_l)\hat{\mathbf{e}}_\nu$ for $j \neq l$. The eigenmodes $\mathbf{v}_\mu$ of $\mathcal{H}$ describe the collective radiative excitations, with complex eigenvalues $\delta_n + \mathrm{i}\upsilon_n$, where δ_n and υ_n denote the collective line shift (from the resonance of the isolated atom) and linewidth, respectively[68]. To determine the occupation of an eigenmode $\mathbf{v}_n$ in the steady-state, we calculate[70] $L_n = |\mathbf{v}_n^{\mathrm{T}}\mathbf{b}|^2/\sum_{n'}|\mathbf{v}_{n'}^{\mathrm{T}}\mathbf{b}|^2$.

Other than the section "Singular defects", we consider ensembles that are weakly interacting where the light-mediated dipole-dipole interactions between the atoms are negligible. The polarisation amplitude dynamics are then approximately given by $\dot{\mathcal{P}}_\mu^{(j)} \approx \mathrm{i}[\Delta_\mu(\mathbf{r}_j) + \mathrm{i}\gamma]\mathcal{P}_\mu^{(j)} + \mathrm{i}\xi\epsilon_0\hat{\mathbf{e}}_\mu^* \cdot \mathcal{E}(\mathbf{r}_j)/\mathcal{D}$, and therefore in the steady-state we obtain $\mathbf{P}(\mathbf{r}) = \epsilon_0\alpha(\Delta_\mu)\boldsymbol{\mathcal{E}}(\mathbf{r})$ as given in the main text. Under spatially dependent applied level shifts, the detunings of the laser frequency from the resonance of the levels in the $J = 0 \to J' = 1$ transition are chosen to be $\Delta_\pm(\mathbf{r}) = 0$ and $\Delta_x(\mathbf{r}) \equiv \Delta_0(\mathbf{r}) = \delta[1 - \exp(-z^2/10w_0^2)]$, where we use the fact that the $m = 0$ quantisation axis lies in the x direction to relabel the last detuning.

Data availability

The data will be available at https://doi.org/10.17635/lancaster/researchdata/504.

Code availability

The code that supports the findings of this study are available upon reasonable request.

Received: 27 September 2021; Accepted: 10 February 2022;
Published online: 14 March 2022

References

1. Thomson, W. 4. On vortex atoms. *Proc. R. Soc. Edinb.* **6**, 94–105 (1869).
2. Volovik, G. E. *The Universe in a Helium Droplet* (Oxford University Press, 2003).
3. Forbes, A., de Oliveira, M. & Dennis, M. R. Structured light. *Nat. Phot.* **15**, 253–262 (2021).
4. Leach, J., Dennis, M. R., Courtial, J. & Padgett, M. J. Knotted threads of darkness. *Nature* **432**, 165–165 (2004).
5. Dennis, M. R., King, R. P., Jack, B., Oholleran, K. & Padgett, M. J. Isolated optical vortex knots. *Nat. Phys.* **6**, 118–121 (2010).
6. Kedia, H., Bialynicki-Birula, I., Peralta-Salas, D. & Irvine, W. T. M. Tying knots in light fields. *Phys. Rev. Lett.* **111**, 150404 (2013).
7. Larocque, H. et al. Reconstructing the topology of optical polarization knots. *Nat. Phys.* **14**, 1079–1082 (2018).
8. Bauer, T. et al. Observation of optical polarization Möbius strips. *Science* **347**, 964–966 (2015).
9. Ozawa, T. et al. Topological photonics. *Rev. Mod. Phys.* **91**, 015006 (2019).
10. Skyrme, T. H. R. A non-linear field theory. *Proc. R. Soc. Lond. A* **260**, 127–138 (1961).
11. Manton, N. & Sutcliffe, P. *Topological Solitons* (Cambridge University Press, 2004).
12. Battye, R. A. & Sutcliffe, P. M. Symmetric skyrmions. *Phys. Rev. Lett.* **79**, 363–366 (1997).
13. Battye, R. A., Manton, N. S., Sutcliffe, P. M. & Wood, S. W. Light nuclei of even mass number in the Skyrme model. *Phys. Rev. C.* **80**, 034323 (2009).
14. Donoghue, J. F., Golowich, E. & Holstein, B. R. *Dynamics of the Standard Model. Cambridge Monographs on Particle Physics, Nuclear Physics and Cosmology* 2nd edn (Cambridge University Press, 2014).
15. Radu, E. & Volkov, M. S. Stationary ring solitons in field theory—knots and vortons. *Phys. Rep.* **468**, 101 – 151 (2008).
16. Volovik, G. E. & Mineev, V. P. Particle-like solitons in superfluid ^{3}He phases. *Sov. J. Exp. Theor. Phys.* **46**, 401 (1977).
17. Shankar, R. Applications of topology to the study of ordered systems. *J. Phys.* **38**, 1405–1412 (1977).
18. Ruostekoski, J. & Anglin, J. R. Creating vortex rings and three-dimensional skyrmions in Bose-Einstein condensates. *Phys. Rev. Lett.* **86**, 3934 (2001).
19. Al Khawaja, U. & Stoof, H. Skyrmions in a ferromagnetic Bose-Einstein condensate. *Nature* **411**, 918–920 (2001).
20. Battye, R. A., Cooper, N. R. & Sutcliffe, P. M. Stable skyrmions in two-component Bose-Einstein condensates. *Phys. Rev. Lett.* **88**, 080401 (2002).
21. Savage, C. M. & Ruostekoski, J. Energetically stable particlelike skyrmions in a trapped Bose-Einstein condensate. *Phys. Rev. Lett.* **91**, 010403 (2003).
22. Ruostekoski, J. Stable particlelike solitons with multiply quantized vortex lines in Bose-Einstein condensates. *Phys. Rev. A* **70**, 041601 (2004).
23. Kawakami, T., Mizushima, T., Nitta, M. & Machida, K. Stable skyrmions in *SU*(2) gauged Bose-Einstein condensates. *Phys. Rev. Lett.* **109**, 015301 (2012).
24. Tiurev, K. et al. Three-dimensional skyrmions in spin-2 Bose–Einstein condensates. *N. J. Phys.* **20**, 055011 (2018).
25. Faddeev, L. & Niemi, A. J. Stable knot-like structures in classical field theory. *Nature* **387**, 58–61 (1997).
26. Battye, R. A. & Sutcliffe, P. M. Knots as stable soliton solutions in a three-dimensional classical field theory. *Phys. Rev. Lett.* **81**, 4798–4801 (1998).
27. Sutcliffe, P. Skyrmion knots in frustrated magnets. *Phys. Rev. Lett.* **118**, 247203 (2017).
28. Hietarinta, J. & Salo, P. Faddeev-Hopf knots: dynamics of linked un-knots. *Phys. Lett. B* **451**, 60–67 (1999).
29. Babaev, E., Faddeev, L. D. & Niemi, A. J. Hidden symmetry and knot solitons in a charged two-condensate Bose system. *Phys. Rev. B* **65**, 100512 (2002).
30. Hall, D. S. et al. Tying quantum knots. *Nat. Phys.* **12**, 478–483 (2016).
31. Lee, W. et al. Synthetic electromagnetic knot in a three-dimensional skyrmion. *Sci. Adv.* **4**, 1–8 (2018).
32. Ackerman, P. J. & Smalyukh, I. I. Diversity of knot solitons in liquid crystals manifested by linking of preimages in torons and hopfions. *Phys. Rev. X* **7**, 011006 (2017).
33. Sugic, D. et al. Particle-like topologies in light. *Nat. Commun.* **12**, 6785 (2020).
34. Borgh, M. O., Nitta, M. & Ruostekoski, J. Stable core symmetries and confined textures for a vortex line in a spinor Bose–Einstein condensate. *Phys. Rev. Lett.* **116**, 085301 (2016).
35. Anderson, P. W. & Toulouse, G. Phase slippage without vortex cores: Vortex textures in superfluid ^{3}He. *Phys. Rev. Lett.* **38**, 508–511 (1977).
36. Chechetkin, V. R. Types of vortex solutions in superfluid He-3. *Zh. Eksp. Teor. Fiz.* **71**, 1463 (1976).
37. Mermin, N. D. & Ho, T.-L. Circulation and angular momentum in the *a* phase of superfluid Helium-3. *Phys. Rev. Lett.* **36**, 594–597 (1976).
38. Mühlbauer, S. et al. Skyrmion lattice in a chiral magnet. *Science* **323**, 915–919 (2009).
39. Nagaosa, N. & Tokura, Y. Topological properties and dynamics of magnetic skyrmions. *Nat. Nanotech.* **8**, 899–911 (2013).
40. Leanhardt, A. E., Shin, Y., Kielpinski, D., Pritchard, D. E. & Ketterle, W. Coreless vortex formation in a spinor Bose–Einstein condensate. *Phys. Rev. Lett.* **90**, 140403 (2003).
41. Leslie, L. S., Hansen, A., Wright, K. C., Deutsch, B. M. & Bigelow, N. P. Creation and detection of skyrmions in a Bose-Einstein condensate. *Phys. Rev. Lett.* **103**, 250401 (2009).
42. Choi, J., Kwon, W. J. & Shin, Y. Observation of topologically stable 2D skyrmions in an antiferromagnetic spinor Bose–Einstein condensate. *Phys. Rev. Lett.* **108**, 035301 (2012).
43. Weiss, L. S. et al. Controlled creation of a singular spinor vortex by circumventing the Dirac belt trick. *Nat. Commun.* **10**, 4772 (2019).
44. Ho, T.-L. Spinor Bose condensates in optical traps. *Phys. Rev. Lett.* **81**, 742–745 (1998).
45. Ohmi, T. & Machida, K. Bose-Einstein condensation with internal degrees of freedom in alkali atom gases. *J. Phys. Soc. Jpn.* **67**, 1822–1825 (1998).
46. Mizushima, T., Machida, K. & Kita, T. Mermin–Ho vortex in ferromagnetic spinor Bose–Einstein condensates. *Phys. Rev. Lett.* **89**, 030401 (2002).
47. Lovegrove, J., Borgh, M. O. & Ruostekoski, J. Energetic stability of coreless vortices in spin-1 Bose-Einstein condensates with conserved magnetization. *Phys. Rev. Lett.* **112**, 075301 (2014).
48. Cilibrizzi, P. et al. Half-skyrmion spin textures in polariton microcavities. *Phys. Rev. B* **94**, 045315 (2016).
49. Donati, S. et al. Twist of generalized skyrmions and spin vortices in a polariton superfluid. *PNAS* **113**, 14926–14931 (2016).
50. Król, M. et al. Observation of second-order meron polarization textures in optical microcavities. *Optica* **8**, 255–261 (2021).
51. Dominici, L. et al. Full-Bloch beams and ultrafast Rabi-rotating vortices. *Phys. Rev. Res.* **3**, 013007 (2021).
52. Tsesses, S. et al. Optical skyrmion lattice in evanescent electromagnetic fields. *Science* **361**, 993–996 (2018).
53. Du, L., Yang, A., Zayats, A. V. & Yuan, X. Deep-subwavelength features of photonic skyrmions in a confined electromagnetic field with orbital angular momentum. *Nat. Phys.* **15**, 650–654 (2019).
54. Gao, S. et al. Paraxial skyrmionic beams. *Phys. Rev. A* **102**, 053513 (2020).
55. Gutiérrez-Cuevas, R. & Pisanty, E. Optical polarization skyrmionic fields in free space. *J. Opt.* **23**, 024004 (2021).
56. Bliokh, K. Y., Alonso, M. A. & Dennis, M. R. Geometric phases in 2D and 3D polarized fields: geometrical, dynamical, and topological aspects. *Rep. Prog. Phys.* **82**, 122401 (2019).
57. Beckley, A. M., Brown, T. G. & Alonso, M. A. Full Poincaré beams. *Opt. Express* **18**, 10777–10785 (2010).
58. Born, M. & Wolf, E. *Principles of Optics* 7th edn (Cambridge University Press, 1999).
59. Jackson, J. D. *Classical Electrodynamics* 3rd edn (Wiley, 1999).
60. Jackiw, R. & Pi, S.-Y. Creation and evolution of magnetic helicity. *Phys. Rev. D.* **61**, 105015 (2000).

61. Ruostekoski, J. & Dutton, Z. Engineering vortex rings and systems for controlled studies of vortex interactions in Bose-Einstein condensates. *Phys. Rev. A* **72**, 063626 (2005).
62. Gerbier, F., Widera, A., Fölling, S., Mandel, O. & Bloch, I. Resonant control of spin dynamics in ultracold quantum gases by microwave dressing. *Phys. Rev. A* **73**, 041602 (2006).
63. Hopf, H. Über die Abbildungen der dreidimensionalen Sphäre auf die Kugelfläche. *Math. Ann.* **104**, 637–665 (1931).
64. Gudnason, S. B. & Nitta, M. Linking number of vortices as baryon number. *Phys. Rev. D.* **101**, 065011 (2020).
65. Berry, M. V. & Dennis, M. R. Knotting and unknotting of phase singularities: Helmholtz waves, paraxial waves and waves in 2+1 spacetime. *J. Phys. A: Math. Gen.* **34**, 8877–8888 (2001).
66. Lopez-Mago, D. On the overall polarisation properties of Poincaré beams. *J. Opt.* **21**, 115605 (2019).
67. Ruostekoski, J. & Javanainen, J. Quantum field theory of cooperative atom response: low light intensity. *Phys. Rev. A* **55**, 513–526 (1997).
68. Lee, M. D., Jenkins, S. D. & Ruostekoski, J. Stochastic methods for light propagation and recurrent scattering in saturated and nonsaturated atomic ensembles. *Phys. Rev. A* **93**, 063803 (2016).
69. Adkins, G. S., Nappi, C. R. & Witten, E. Static properties of nucleons in the Skyrme model. *Nuc. Phys. B* **228**, 552–566 (1983).
70. Facchinetti, G. & Ruostekoski, J. Interaction of light with planar lattices of atoms: Reflection, transmission, and cooperative magnetometry. *Phys. Rev. A* **97**, 023833 (2018).

Acknowledgements

C.D.P. and J.R. acknowledge financial support from the UK EPSRC (Grant Nos. EP/S002952/1, EP/P026133/1), and M.R.D. from the EPSRC Centre for Doctoral Training in Topological Design (EP/S02297X/1).

Author contributions

C.D.P. and J.R. formulated the theory with assistance from M.R.D. C.D.P. performed the numerics. C.D.P., M.R.D., and J.R. wrote the manuscript.

Competing interests

The authors declare no competing interests.

Additional information

Correspondence and requests for materials should be addressed to Christopher D. Parmee or Janne Ruostekoski.

Peer review information *Communications Physics* thanks Lorenzo Dominici, Witold Bardyszewski, Amir Rahmani and the other, anonymous, reviewer(s) for their contribution to the peer review of this work.

Reprints and permission information is available at http://www.nature.com/reprints

Publisher's note Springer Nature remains neutral with regard to jurisdictional claims in published maps and institutional affiliations.